Version of Record: https://www.sciencedirect.com/science/article/pii/S0376738817310876
Manuscript_2811bb85f90c3131c1e2dcf2d6a1478a

Spray-Painted Graphene Oxide Membrane Fuel Cells

T. Bayer[1,2*], R. Selyanchyn[1], S. Fujikawa[1], K. Sasaki[1-4] and S. M. Lyth[1,5]

[1] International Institute for Carbon-Neutral Energy Research (WPI-I2CNER), Kyushu University, 744 Motooka, Nishi-ku, 819-0395, Fukuoka, Japan

[2] Next-Generation Fuel Cell Research Center (NEXT-FC), Kyushu University, 744 Motooka, Nishi-ku, 819-0395, Fukuoka, Japan

[3] International Research Center for Hydrogen Energy, Kyushu University, 744 Motooka, Nishi-ku, 819-0395, Fukuoka, Japan

[4] Department of Mechanical Engineering, Kyushu University, 744 Motooka, Nishi-ku, 819-0395, Fukuoka, Japan

[5] Energy2050, Department of Mechanical Engineering, University of Sheffield, S10 2TN, UK

[*] Corresponding author, bayer.thomas.905@m.kyushu-u.ac.jp

Abstract

Graphene Oxide (GO) is potentially a useful electrolyte material for polymer electrolyte membrane fuel cells due to its high strength, excellent hydrogen gas barrier properties, hydrophilicity, and proton conducting acidic functional groups. Here, GO paper is prepared from aqueous dispersion by vacuum-filtration, and the hydrogen permeability ($2x10^{-2}$ barrer) is measured to be 3 orders of magnitude lower than Nafion (30 barrer) at 30°C. The in-plane and through-plane conductivities are measured to be 49.9 and 0.3 mS cm^{-1}, respectively. This significant anisotropy is attributed to the lamellar structure of GO, and the physical anisotropy between the thickness and lateral size of the GO nanoplatelets. Interestingly, the in-plane conductivity of GO is comparable to the through-plane conductivity of Nafion. GO membrane fuel cells (GOMFCs) are fabricated. To compensate for the low in-plane conductivity of GO, whilst taking advantage of the excellent hydrogen gas barrier properties, extremely thin electrode-supported GOMFCs are prepared by spray painting GO directly onto the electrocatalyst layer. The effect of membrane thickness on cell performance is investigated. Decreasing membrane thickness by spray painting improves the power density from 3.7 mW cm^{-2} for a 50 µm-thick membrane-supported GOMFC, to 79 mW cm^{-2} for a 3 µm-thick, spray-painted membrane, electrode-supported GOMFC.

Keywords: Graphene Oxide, Proton Conduction, Hydrogen Energy, Spraying, Membranes, Green Chemistry

1 Introduction

Finite fossil fuel energy reserves and increasing energy demand have led to greater interest in efficient energy conversion devices. Fuel cells provide electricity efficiently and cleanly, and are already commercially available as stationary systems (e.g. Ene-Farm, the Japanese micro-combined heat and power system), portable systems for auxiliary power or consumer electronics (e.g. Upp, the USB charging unit from Intelligent Energy), and in fuel cell vehicles (e.g. the Toyota Mirai) [1]. Polymer electrolyte membrane fuel cells (PEMFCs) are one of the most commercially viable types of fuel cell, due to relatively low operation temperature, dynamic load response, and simplicity [2,3]. A key component is the ionomer membrane, typically Nafion, consisting of a fluorinated carbon backbone with perfluoro- side chains terminating in sulfonic acid groups. This material exhibits high proton conductivity (> 0.1 S cm^{-1}), has good mechanical properties, and currently dominates the PEMFC market.

However, Nafion is expensive, and also limits PEMFC operation to ~80°C, due to the reliance on hydration for proton conductivity. Dehydration decreases the conductivity, and leads to membrane swelling or shrinkage, causing deterioration of the electrolyte-electrocatalyst interface [4]. The mechanical stability of Nafion is reduced at high temperature due to low glass transition temperature (~ 110°C) [5–8]. Fuel crossover dramatically increases with decreasing membrane thickness and increasing operation temperature, leading to decreased fuel cell performance [9,10]. Finally, membrane degradation is caused by H_2O_2 radicals, inhibiting the use of non-precious catalysts [11,12]. To reduce the cost and improve the performance of PEMFCs, new membrane materials with high strength, good hydrogen gas barrier properties, and high hydrophilicity are desirable.

Graphene oxide (GO), which is obtained by chemical functionalization and exfoliation of graphite, is receiving attention due to its facile dispersion in water [13], electronically insulating properties [14], thermal conductivity [15], and gas barrier properties [16]. The oxygen-containing functional groups on the

surface of GO include carboxylic, hydroxyl, epoxy and carbonyl groups (Figure 1a) [17,18], resulting in hydrophilicity, good dispersibility in water, and low pH. It is produced at increasingly large scale and the price is dropping rapidly. GO dispersions can be easily processed into single layer, few-layer, or multilayer films by screen printing, inkjet printing, spin-coating, spraying, or dip-coating. Strong and flexible free-standing multilayer GO paper can be manufactured by bar coating, or vacuum filtration [19]. Unimpeded motion of water monolayers through the two-dimensional capillaries formed between GO sheets has been reported [20], whilst the free and chemically bound water interlayers have been reported be completely removed in vacuum [21].

The acidic carboxylic acid groups in GO contribute to its proton conductivity [22–25], suggesting that GO can be utilized as an ionomer membrane in PEMFCs. Kumar et al. reported a temperature-dependent through-plane conductivity for GO of between 41 and 82 mS cm^{-1} (100% relative humidity (RH), 25 to 90°C) [26]. In-plane conductivity between 10^{-4} and 10^{-2} mS cm^{-1} (100% RH, 20 to 80°C) was reported for GO by Zarrin et al. [27]. They also showed that the conductivity of GO can be increased by chemical modification, and reported sulfonated GO with an in-plane conductivity of 100 to 200 mS cm^{-1} (100% RH, 20 to 80°C). Tateishi et al. reported maximum through- and in-plane conductivities between 10^{-3} and 10^{-1} mS cm^{-1} at 25°C and 95% RH [28]. Hatakeyama et al. investigated the in-plane conductivity of mono-layer GO flakes and multilayer GO papers. They reported that the in-plane conductivity of GO increases with increasing membrane thickness, with a maximum value of ~1 mS cm^{-1} at 25°C and 90% RH [29]. Recently, our group determined that GO is actually a mixed ionic-electronic conductor (MIEC), the proportion of ionic to electronic conduction depending on the level of humidification [30]. Using impedance spectroscopy and blocking layer measurements, we showed that electronic conductivity is dominant in "dry" conditions below 40% RH. Based on the activation energies (i.e., 0.05 to 0.88 eV, depending on temperature and RH) proton transport was determined to occur via a Grotthuss-type mechanism at lower temperatures, and via a vehicle or surface proton hopping mechanism at higher temperature (>60°C). A large body of work has been published on the use of GO in polymer composites with common ionomers. For example, Kumar et al. reported improved performance compared to Nafion for a 4 wt% GO/Nafion composite at 100°C [31]. Jiang et al. reported that the incorporation of sodium dodecylbenzene sulfonate-adsorbed GO in sulfonated poly ether ether ketone (SPEEK) increased the ion-exchange capacity, water

uptake and proton conductivity, whilst reducing methanol permeability [32]. Xu et al. reported a maximum cell power density of 600 mW cm^{-2} at 175 °C for a polybenzimidazol (PBI) / sulfonated GO composite membrane [33]. Bao et al. reported polyvinyl alcohol (PVA) / GO nanocomposites [34]. Shukla et al. reported sulfonated graphene nanoribbons prepared by unzipping and sulfonation of multi-walled carbon nanotubes, and incorporated them into a SPEEK matrix. For this composite membrane a maximum power density of 660 mW cm^{-2} at 60°C and 100% RH was reported [35]. The above studies essentially conclude that GO improves performance due to improved hydrophilicity and fuel barrier properties. However, in those cases it is difficult to separate the different ionic contributions of GO and the polymer ionomer.

The use of PEMFC membranes consisting primarily of multilayer GO has also been investigated, but to a much lesser extent. Tateishi et al. first reported the performance of a fuel cell using a pure GO paper membrane, with maximum power density of ~13 mW cm^{-2} at room temperature [28]. Scott et al reported a freestanding sulfonated GO paper membrane achieving a GOMFC power density of 113 mW cm^{-2} at 40 °C [22]. Gao et al reported an ozonated GO membrane fuel cell with through-plane conductivity of around 2 mS cm^{-1} and current densities of up to 0.55 A cm^{-2}, with a power density of ~160 mW cm^{-2} [36]. Sulfonic acid-functionalized GO with a ionic conductivity of 58 mS cm^{-1} at 55°C has been reported as an electrochemical gas sensor for ethanol detection (with sensitivity of 25 ppm)s [37].

In our own previous work, GO membranes have been intensively characterized for application in fuel cells. The mechanical properties are relevant to membrane handling, membrane electrode assembly (MEA) preparation and cell longevity. We measured the tensile strength of GO to be 54.5 MPa, compared with 30.7 MPa for Nafion, indicating that GO is very strong [38,39]. The proton conductivity in GO is attributed to water-mediated ion transport mechanisms (e.g. the Grotthuss mechanism) [40,41], and therefore we measured the water uptake and swelling of GO to be 31.1 wt% and 18.7 %, respectively, for GO, compared with 25.6 wt% and 16.0 %, respectively, for Nafion [39]. The expansion and contraction of GO membranes with changes in relative humidity was investigated by in-situ environmental scanning electron microscopy (ESEM), and electron energy loss spectroscopy (EELS), and signals for water ice were detected even after drying under high vacuum conditions, indicating the extremely strong affinity between GO and water [42]. We revealed that GO should be considered a mixed ionic-electronic conductor by aid of impedance

spectroscopy and ion blocking layer measurements [30]. The proton conductivity was 0.5 mS cm^{-1} at 90°C and 100% RH, and decreased with humidity, as expected for water-mediated conduction mechanisms. However, below 40% RH, a strong *increase* in conductivity was observed, due to the increasing contribution from electrons. The permittivity also increased significantly with decreasing humidity. Finally, we reported a fuel cell utilizing GO paper in place of Nafion, achieving a power density of 35 mW cm^{-2} at ambient temperature, as well as identifying key membrane degradation mechanisms related to thermal and electrochemical reduction of the membrane [39].

One method to improve cell performance is by decreasing the membrane thickness, in order to reduce the membrane resistance, translating to an increase in the power density. However, ionomer materials become fragile and more difficult to handle the thinner they get, and we have found that GO membranes less than 10 µm in thickness break easily during MEA fabrication. Therefore for thinner electrolytes, the electrode-supported preparation method is strongly recommended, in which ionomer is deposited from dispersion (or solution) directly onto the electrode. Klingele et al. first reported the novel fabrication method in which a thin layer Nafion (8-25 µm) was ink-jet printed onto the anode and cathode by "direct membrane deposition" (DMD) before assembling the two parts into an MEA. Extraordinarily high power density was achieved (4 W/cm^2 using pure H_2/O_2) as a result of reduced membrane resistance and improved contact resistance between the membrane and catalyst layer [43]. We reported the fabrication and evaluation of a similar electrode-supported PEMFC design. In this case, a thin layer of Nafion (~10 µm) was spray-painted directly onto the cathode gas diffusion electrode (GDE). The anode electrocatalyst was then spray-painted on top of this to complete the membrane electrode assembly (MEA). A power density of 580 mW cm^{-2} was achieved (80°C, H_2/air), ~33% higher than the 50 µm Nafion reference membrane. However, the open circuit voltage (OCV) was very low, which was attributed to cracks in the microporous layer (MPL) of the carbon paper GDE, leading to pinholes in the spray-pained membrane and increased hydrogen crossover [44]. Recently we reported a fully sprayed Aquivion-based PEMFC with high power density at H_2/air operation (10 µm thick membrane, 1.6 W cm^{-2} at 300 kPa_{abs}) [45]. We showed that the incorporation of a GO/cerium oxide interlayer supressed electrical shorting and reduced hydrogen gas crossover to ~1 mA cm^{-2}, surpassing the DOE hydrogen crossover targets for 2020.

Here we report new results in which the proton conductivity of GO is investigated in further detail, and the anisotropy between the in-plane and through-place conductivity is investigated. The hydrogen permeability is measured. The effect of membrane thickness on the cell performance is investigated by spray-painting GO membranes from water ethanol dispersion.

2 Experimental

2.1 GO Membrane preparation

GO dispersions were obtained from Graphene Supermarket (highly concentrated GO dispersion in water, Hummers synthesis method). The nominal concentration (5 g/L), carbon content (79 at%), oxygen content (20 at%), flake size (0.5 to 5 µm), and thickness (1 atomic layer - at least 60%, corresponding to a thickness of ~0.7 nm) were provided by the manufacturer [46,47]. Free-standing multilayer graphene oxide paper was prepared by vacuum-filtration of the dispersion onto Millipore filters (PTFE, 35 mm diameter, pore size 0.025 µm). The GO retentate was dried at room temperature for 48 hours and then peeled-off the filter. The resulting membrane is photographed in Figure 1d.

2.2 Morphological and chemical characterization

The morphology was investigated by scanning electron microscopy (SEM, *Hitachi S-5200*, 30kV) and laser microscopy (*Olympus LEXT 3d OLS 4000)*. The chemical composition was determined by X-ray photoelectron spectroscopy (XPS, *KRATOS Analytical ESCA-3400,* Mg Kα radiation, 12 kW, 10mA). X-ray diffraction (XRD) was measured using a Smartlab X-ray Diffractometer with Cu Kα radiation.

2.3 Water uptake measurement

Water uptake and swelling were measured on samples with a size of 10 x 10 mm. Five samples of each different material were measured for reproducibility. Samples were first dried in vacuum at 60°C for two hours. The mass was then immediately determined using an analytical balance (Mettler Toledo, ± 0.1 mg) and the thickness was determined using a micrometer (Mitutoyo, ± 1 µm). Samples were then placed into a water bath at room temperature for one hour. After saturation, excess surface water was removed carefully

with tissue paper, and the mass and thickness were measured again. Water uptake (WU) was calculated using Equation 1, where m_{wet} and m_{dry} are the wet and dry masses, respectively:

$$WU\ (\%) = \frac{m_{wet} - m_{dry}}{m_{dry}} \cdot 100\% \quad [1]$$

Swelling (Sw) was calculated by using Equation 2, where T_{wet} and T_{dry} are the wet and dry thicknesses of the samples, respectively:

$$Sw\ (\%) = \frac{T_{wet} - T_{dry}}{T_{dry}} \cdot 100\% \quad [2]$$

2.4 Gas permeance measurement

For gas permeance measurements, the membrane area was masked with Kapton and alumina tape, leaving a circle of d = 1 cm, and an area of S = 0.785 cm^2. To prevent deformation during measurements and provide mechanical support, the membranes were placed on a porous polycarbonate filter (1.2 μm pore size). The permeation rate of dry hydrogen through GO and Nafion 212 membranes was measured between room temperature and 80 °C using a GTR-11A/31A gas barrier testing system (GTR Tec Corp., Japan). This system uses a differential-pressure method where gas permeation is induced by vacuum on the permeate side and extra pressure applied at the feed side. This method is described in more detail in our previous studies [48]. The total pressure difference was 200 kPa. The sample collection time after vacuuming the permeate side of the membrane was 30 min. The collected gas was transferred to a gas chromatograph, and the total volume of resulting gas was measured. The gas chromatograph was combined with a thermal conductivity detector (TCD, Yanaco G3700T, Japan).

2.5 Proton conductivity measurements

Ionic conductivity was investigated for a range of temperatures and relative humidity (RH) using a membrane testing system (MTS-740, Scribner) coupled with an impedance analyser (Solatron SI1260) [49]. Through-plane conductivity was investigated by using a dedicated electrode setup, as described in more detail in our previous work [30]. GO and Nafion membranes were measured with an AC amplitude of 10

mV in a frequency range from 30 MHz to 10 Hz, from 30 to 90°C. Before measurements, the samples were pre-treated at 100% RH for 4 h. Conductivity (σ) was calculated using Equation 3, using the membrane thickness (T, cm), membrane resistance (R, Ω) and the cross-sectional area (A, 0.5 cm^2) [39].

$$\sigma = \frac{T}{R \cdot A} \quad [3]$$

In-plane conductivity was also measured using the *MTS-740* system, using an alternative in-plane measurement electrode setup [49]. Samples with dimensions of 5 x 30 mm and a thickness of 18 µm (GO) and 50 µm (Nafion) respectively were measured in the frequency range of 30 MHz to 10 Hz with an AC amplitude of 10 mV. The impedance was measured from 30 to 90°C at an RH of 100%. Before impedance measurements, each sample was pre-treated for 4 h. The in-plane conductivity (σ_{IP}) was calculated using Equation 4, in which L is the distance between the two platinum electrodes (5 mm), R is the measured resistance, and A_{CS} the cross-sectional area of the sample (0.09 mm^2 for GO and 0.25 mm^2 for Nafion):

$$\sigma_{IP} = \frac{L}{R \cdot A_{CS}} \quad [4]$$

2.6 Fuel cell fabrication and testing

Membrane-supported and electrode-supported membrane electrode assemblies (MEAs) were both fabricated. An automated Nordson K.K. spraying device with an A7A spray gun, a nozzle diameter of 0.5 mm, and a hot stage was used to deposit electrocatalyst layers and/or electrolyte layers, as required. The fabrication process is described in detail in our previous work [44]. Electrocatalyst ink was prepared by mixing Pt/C electrocatalyst (Tanaka Kikinzoku Kogyo K.K., 46.2 wt% Pt) with 5 wt% Nafion® solution (Wako, Japan), ethanol (Chameleon, Japan), and deionized water. The mass ratio of Nafion to Pt/C was 0.28:0.72. All loadings were calculated after drying, using an analytic balance (Mettler Toledo, ± 0.1 mg). Conventional electrolyte-supported MEAs were fabricated by spraying electrocatalyst (electrode area 0.5 cm^2, Pt loading 0.3 mg_{Pt} cm^{-2}) directly onto both sides of a Nafion®212 membrane using a polyethylene terephthalate (PET) mask, at 65°C. Microporous layer (MPL)-coated gas diffusion layers (GDLs, Sigracet®

25 BC) were precisely positioned over the electrocatalyst layers and then fitted into a cell holder (NEDO cell, 1 cm^2 flow field area, 2 N compression) for electrochemical testing. Electrode-supported MEAs were fabricated using a 4 x 4 cm MPL-coated GDL (Sigracet® 25 BC) as mechanical support for the fuel cell. Electrocatalyst ink (0.3 mg_{Pt} cm^{-2}) was first sprayed directly onto the MPL with an area of 0.5 cm^2, using a PET mask to form the cathode. Subsequently, a mixture of GO dispersion (10 ml) and ethanol (50 ml, Chameleon, Japan) was directly sprayed onto the GDL and electrocatalyst layer over an area of 36 x 36 mm (12.96 cm^2) in 4 passes, following a serpentine pathway. This ensured complete and uniform coverage of the GDL and electrocatalyst layer. A video of the spraying process can be found in Supplementary Information. The average thickness of the sprayed electrolyte was calculated from the mass loading and density of GO (1.44 g cm^{-3}, calculated). The device was again masked, and then the anode electrocatalyst layer was sprayed (0.5 cm^2, 0.3 mg_{Pt} cm^{-2}) directly above the cathode. Finally, a GDL was placed over the anode, and the MEA was fitted into the cell holder. The MEAs were made significantly larger than the flow-field in order to improve sealing in this particular cell. For comparison a Nafion-based MEA was prepared by depositing electrocatalyst with the same loading onto a Nafion membrane (Nafion®212, 50 µm thickness) using the same electrode size, catalyst loading, and without hot-pressing as described in our previous work [39]. All fuel cells were maintained at 30°C during measurement. Hydrogen and air were flowed at 100 ml min^{-1} and 95% RH. The cell performance was investigated using a potentiostat (*VersaSTAT 4, Amtek*).

3 Results and discussion

3.1 Morphology and chemical composition

Figure 1b shows a photograph of a large GO membrane, highlighting that the size is essentially arbitrary, and that GO membranes are free-standing, flexible, and strong enough to be handled. Figure 1c shows an SEM image of a GO membrane cross-section. A slightly corrugated surface is observed and the multilayer nature of the membranes is clearly visible. Figure 1d shows the surface topology as obtained from laser microscopy (the x-direction is magnified to emphasize the surface microstructure). The surface roughness is 0.50 (± 0.03) µm for the upper side of the membrane (which was dried in contact with air) and 0.18 (±

0.01) µm for the underside (which dried in contact with the PTFE filter). This difference is attributed to the surface tension at the surface during drying, and the templating effect of the extremely smooth PTFE membrane. For comparison, the surface roughness of Nafion is 0.052 (± 0.01) µm.

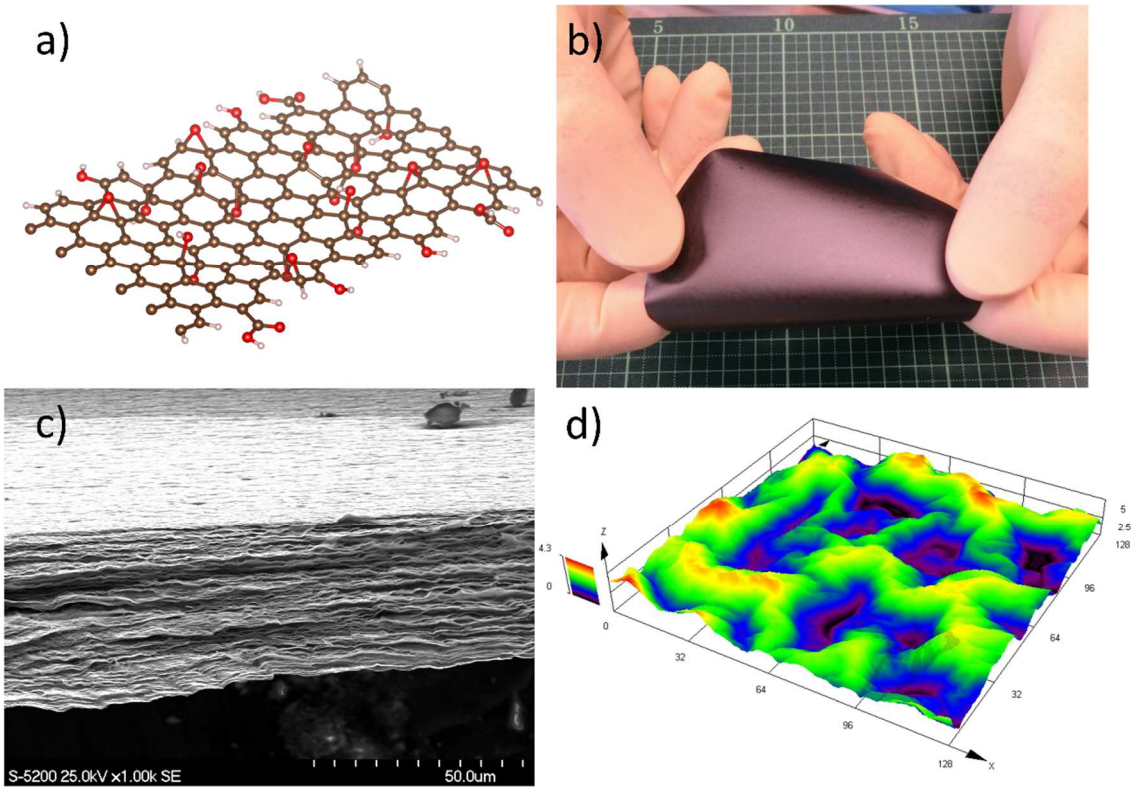

Figure 1. a) Theoretical chemical structure of GO [50]. *b) Freestanding GO membrane. c) SEM image of the cross-section of a GO membrane. d) Laser microscopy image showing the rough surface structure of GO membranes.*

The oxygen content of the GO membranes was determined by XPS to be 20.9 at% (Figure 2), corresponding to a carbon content of 79.1 at%. No other major peaks were detected. The oxygen is attributed (via deconvolution of the C1s and O1s signals) to epoxy, hydroxyl, carbonyl, and carboxyl functional groups attached to sp^3 hybridized C-C bonds in the carbon backbone of GO, as well as adsorbed water (Figure 2b-c). The interlayer spacing was determined by XRD under ambient conditions to be 0.76 nm (Figure 2d), which is more than twice that of graphite (0.34 nm), due to the presence of the surface oxygen groups and intercalated water.

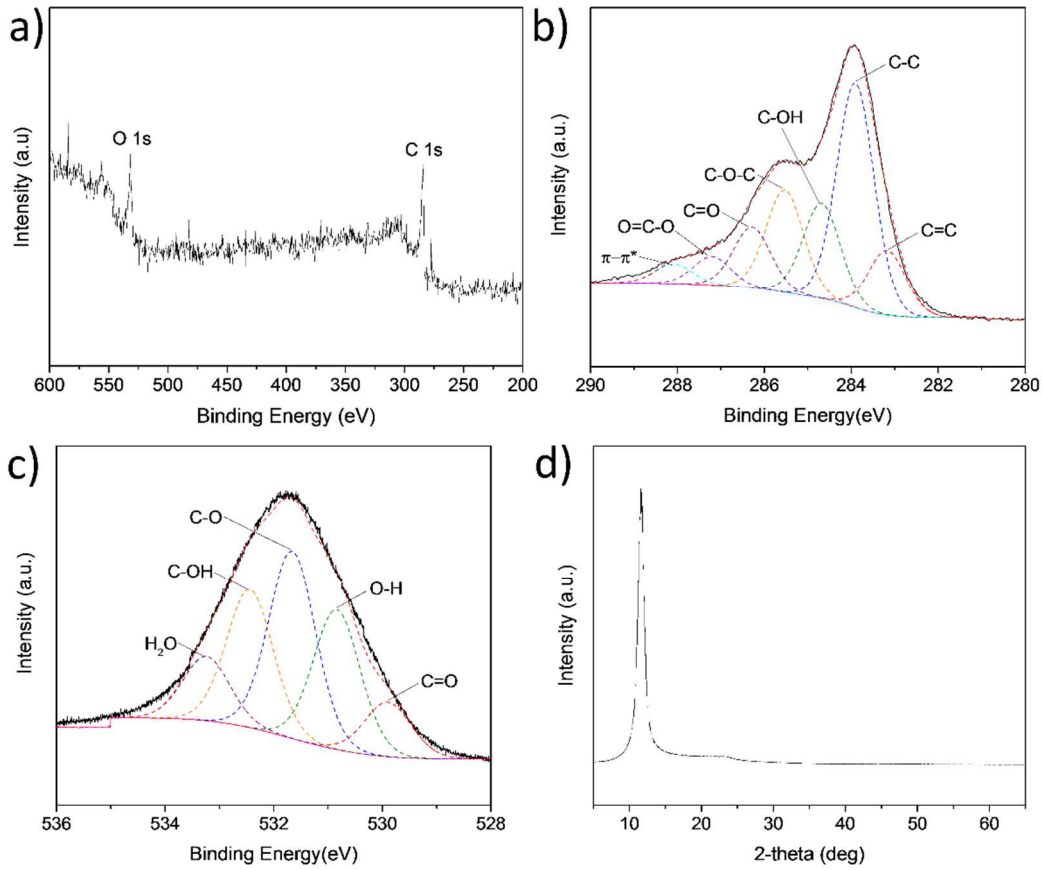

Figure 2. a) XPS wide scan spectrum of graphene oxide (GO). b) C 1s and c) O 1s spectra with component analysis. d) XRD pattern of GO under ambient conditions.

3.2 Tensile Strength, Water uptake and swelling

The tensile strength of GO was measured in our previous work to be 54.5 ± 3.3 MPa, approximately twice that of Nafion (30.7 ± 0.4 MPa) [39]. Water uptake and swelling measurements were performed because the change in physical dimensions with increasing humidity, and the corresponding strain, can impact fuel cell performance and durability under operation. For example, excessive swelling may lead to deterioration of the membrane-electrocatalyst interface, or membrane failure [4]. After immersion in water, the GO membrane visibly swelled, becoming extremely fragile and resembling a hydrogel-type structure. The water uptake of GO (325.6 ± 22.1 wt%) is approximately 20 times higher than that of Nafion (15.4 ± 0.6 wt%). Through-plane swelling is dominant, with a strong increase in thickness. However the swelling in-plane was negligible. Through-plane swelling was 197.8 ± 39.4% for GO, also around 20 times higher than that of Nafion (10.4 ± 1.1%). The higher water uptake in GO indicates a larger driving force for water absorption

and suggests that the GO membrane could maintain proton conductivity even under low humidity conditions. However, in our previous work we observed mixed ionic-electronic conductivity in GO membranes, with a strong increase in electronic conductivity with decreasing humidity [30]. For this reason graphene oxide membrane fuel cells are investigated here at high humidity. However, Kumar et al. reported strongly increased fuel cell performance for GO/Nafion composite membranes compared to recast Nafion at 120°C and 25% RH (i.e. 212 vs 56 mW/cm^2), rationalised by increased water retention by GO and the associated proton conductivity [31]. On the other hand, the greater degree of swelling in GO may increase the risk of deterioration of the membrane-catalyst interface under fuel cell humidification [4].

3.3 Hydrogen permeance

Previously, hydrogen crossover has been measured to be negligible through GO membranes [48]. In our approach, we use a standard polymer membrane gas permeation set-up, compliant with ISO 15105-1/JIS K7126, with a pressure differential of 200 kPa and detection by gas chromatography. Figure 3 shows the hydrogen gas permeability through GO and Nafion membranes, and the dependence on temperature. The hydrogen permeability of GO is approximately three orders of magnitude lower than that of Nafion. At 30°C, the hydrogen gas permeability of GO is ~1.5x10^{-19} m^3 (STP) m m^{-2} s^{-1} Pa^{-1} (2x10^{-2} barrer) compared with 2x10^{-16} m^3 (STP) m m^{-2} s^{-1} Pa^{-1} (30 barrer) for Nafion. The R^2 values are extremely high, reflecting the low degree of error using this technique. For both samples, the permeability increases with increasing temperature, which is typical behaviour for organic polymers [51], and confirms that the permeability through GO is due to the fundamental properties of the membrane rather than e.g. pinholes or leaks. Permeability is a product of the diffusion and solubility coefficients, and since this increases with temperature it is concluded that the increase in diffusion with temperature is faster than the decrease in hydrogen solubility in the material. These results show that the hydrogen gas permeability of GO is extremely low, but non-negligible. However, this contradicts results reported by Nair et al, in which it was claimed that GO is completely impermeable to hydrogen gas [16]. This discrepancy could be related to the fact that the pressure differential in this case is 20 times higher than used in their experiments, resulting in greater accumulation and easier detection of hydrogen gas after passing through the membrane. In addition, the relative humidity and/or oxygen content is also expected to affect the gas permeability by altering the interlayer distance between GO sheets, which is likely to be different between these two experiments. The

gas permeability of various gases through GO has been previously shown to decrease with increasing humidification. This counter-intuitive result is attributed to the blocking effect of intercalated water molecules between the GO interlayers [52]. However, due to the strong swelling at high RH, the hydrogen permeability could be increased under these conditions. Therefore, further experiments are required in the future to confirm the hydrogen permeability at high humidification. The superior gas barrier properties of GO are expected to result in reduced crossover and higher OCV in MEAs, as compared to Nafion. This could also lead to applications as a barrier layer prevent embrittlement in hydrogen storage systems, or pipelines.

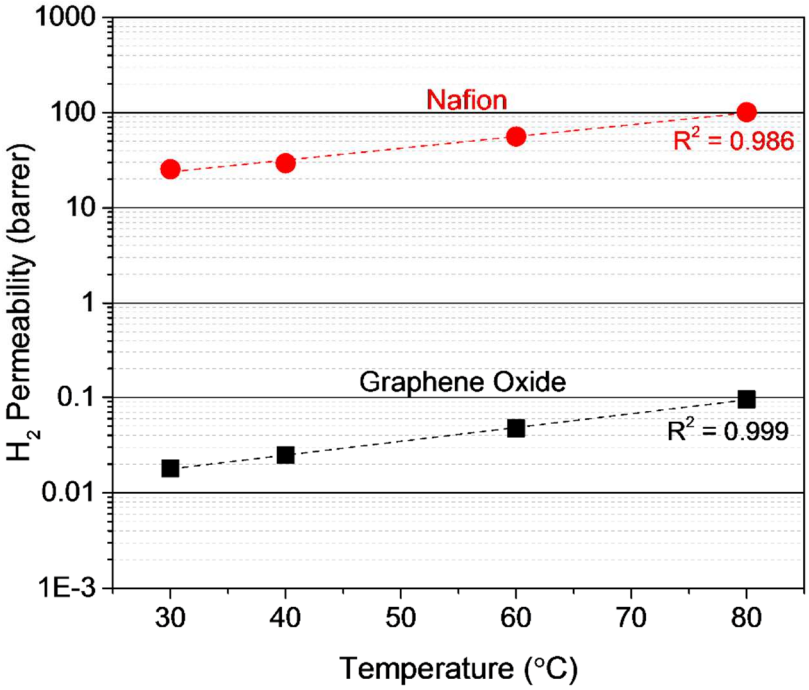

Figure 3. Dependence of hydrogen permeability on temperature for graphene oxide and Nafion. Dashed lines are linear fits of the measurement data.

3.4 In- and through-plane proton conductivity

The proton conductivity is probably the most important characteristic of any ionomer material used in PEMFCs. In many cases, the ionic conductivity reported for ionomer materials in the literature is measured in-plane, sometimes through-plane, and often no distinction is even made. However, in PEMFCs, it is the

through-plane conductivity that governs performance, and this parameter is thus most important. GO in particular is a material with extremely large anisotropy between the nanometer-scale thickness and the micron-scale platelet area. In order to determine if this physical anisotropy is reflected in the proton conductivity, we measured both the in-plane (σ_{IP}) and through-plane (σ_{TP}) conductivity at constant humidity (100%), from 30 to 90°C, using impedance spectroscopy. Figure 4a shows the in-plane and through-plane conductivity for GO and Nafion at different temperatures. The R^2 values calculated from linear fits are very low, reflecting low error in the measurements. The in-plane conductivity of GO ranges from 31.4 to 49.8 mS cm^{-1} between 30 and 70°C, respectively. This is around two orders of magnitude higher than the through-plane conductivity, which ranges from 0.23 to 0.50 mS cm^{-1}. The averaged anisotropy in conductivity is $\sigma_{IP}/\sigma_{TP} = 155$. In contrast, the in-plane conductivity of Nafion ranges from 80.8 to 253.9 mS cm^{-1}, which is only slightly higher than the through-plane conductivity, which ranges from 26.8 to 82.3 mS cm^{-1}. The averaged anisotropy in conductivity of Nafion is just $\sigma_{IP}/\sigma_{TP} = 2.9$. This is in agreement with the literature, in which values range from $\sigma_{IP}/\sigma_{TP} = 1.8$ to 5 are reported [53–55]. The anisotropy in conductivity for GO has not previously been measured in the literature to the best of our knowledge. Above 70°C a slight decrease in the in-plane conductivity of GO is observed. This may be due to reduced water uptake at elevated temperature, as suggested in our previous work [30], resulting in a discontinuous hydrogen-bonding network, and missing water bridges for surface hopping along functional groups.

The extremely high anisotropy in conductivity for GO is attributed to the physical dimensions of the individual GO sheets, and the highly lamellar structure. It is postulated that through-plane proton conduction in GO occurs via an extremely tortuous route through the interlayers and is blocked by the physical presence of the carbon backbone; protons must repeatedly hop from one water molecule to another or from one GO layer to the next in a tortuous route via pores, defects and edges [36]. In contrast, in-plane conduction happens extremely quickly along the dense in-plane hydrogen-bonding network of the water interlayer, or the surface, enabling fast proton transport with no physical barriers.

The minimum activation energy for the Grotthuss-type conduction mechanism (i.e. the energy required to break a hydrogen bond) is generally accepted to be ~0.11 eV [41]. The in-plane and through-plane activation energies obtained from the gradient of the fits in Figure 4 for Nafion are similar (0.19 and 0.17

eV, respectively). These values are typical for Grotthuss-type transport, and are in agreement with the literature. On the other hand, the activation energies for in-plane and through-plane conductivity of GO are 0.10 and 0.13 eV, respectively. These are significantly lower than for Nafion (0.17 and 0.19 eV), and surprisingly of the same order as the minimum energy requirement to break the hydrogen bonds. This is still consistent with a (extremely efficient) Grotthuss-type mechanism, but may also signify an additional conduction mechanism. This could be fast transport of protons through nano-confined channels, as previously postulated in the literature [56–58]. Alternatively, water has been observed to pass almost unimpeded through GO thin films [16]. This may also mean that e.g. hydronium, Zundel, and/or Eigen cations can pass through GO with minimal energy input, significantly reducing the activation energy of the vehicular mechanism. However, despite the low activation energy, the conductivity is still lower than in Nafion, suggesting a significantly lower number of charge carriers. The through-plane activation energy in GO is slightly higher than the in-plane activation energy. This could be due to the tortuous pathway that cations must travel through in the through-plane case. It may also be the case that there is an extra energy barrier for hopping between GO nanoplatelets which manifests as an increase in activation energy.

Significantly, the fast in-plane conductivity of GO is similar in magnitude to the through-plane conductivity of Nafion (~50 mS cm^{-1}). It is therefore clear that removing the tortuous pathway in actual fuel cells could make GO highly competitive as a proton conductor. This is a major engineering challenge at present, and is under further investigation. Currently we are investigating the impact of flake size on the tortuosity and through-plane proton conductivity. These results will be published in our next manuscript, and are therefore not discussed here. Increasing the through-plane conductivity of GO by chemical surface modification e.g. sulfonation or ozonation [22,27,36], might be a more straight forward approach to increase the through-plane proton conductivity.

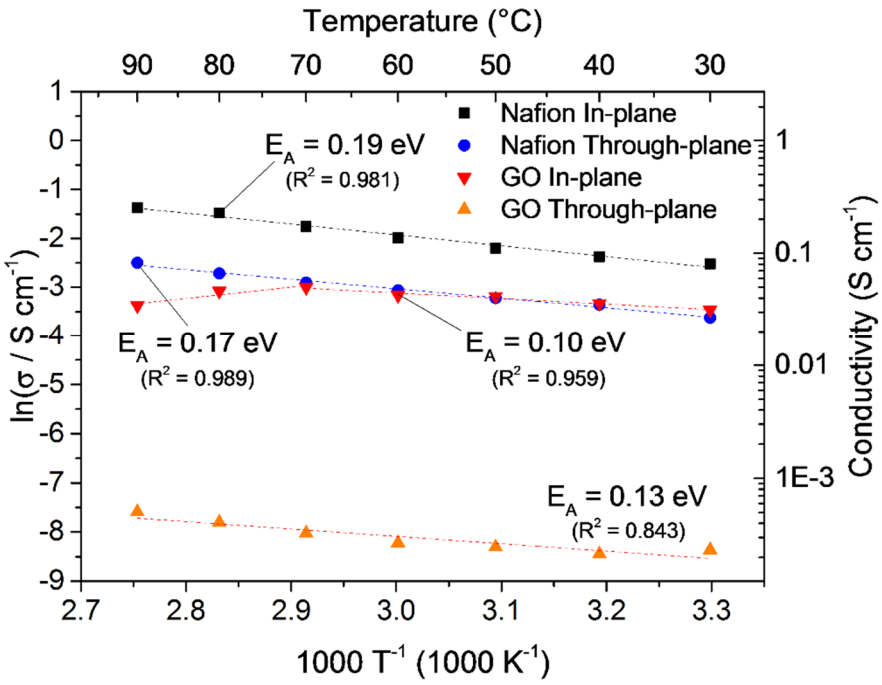

Figure 4. Arrhenius plot of the in-plane and through-plane conductivity of Nafion and GO at 100% RH. Dashed lines are linear fits from which the slope yields the activation energy.

3.5 Fuel cell characterization

It is evident that the relatively low through-plane proton conductivity of GO will be a major limiting factor in the fabrication of fuel cells based around this material. However, the extremely low hydrogen permeability means that fabrication of very thin GO membranes for fuel cells may be possible. This would reduce the reliance on high proton conductivity, as the membrane resistance would be significantly reduced. Therefore, we assembled GO membranes of different thickness into MEAs to test the fuel cell performance. Figure 5 (a-b) shows photographs of an electrolyte-supported GOMFC. This has a structure much like conventional Nafion-membrane based PEMFCs. Figure 5(c-e) shows a series of photos of the fabrication steps of a spray-painted, electrode-supported GOMFC. Photos taken at different points during the ionomer spraying process (Figure 5c) show the carbon support with sprayed cathode electrocatalyst layer, and then the electrolyte membrane getting thicker with each successive GO spraying pass. The final GO ionomer layer is extremely uniform over the entire area of the device. After deposition of the ionomer layer, the anode electrocatalyst is sprayed using a mask (Figure 5d) and finally a carbon paper GDL is attached (Figure 5e).

The surface of the sprayed MEA was investigated at higher magnification by laser microscopy. Images of the anode support and the GO surface are shown in Figure 5 (f-g). The microporous layer (MPL) in the anode gas diffusion layer contains cracks around 30 µm wide, and hundreds of micrometres in length. After spraying GO, the surface microstructure is much more complex than for the thicker vacuum filtered membranes shown in Figure 1. Multiple depressions are observed, potentially corresponding to pinholes, and/or incomplete coverage of the cracks in the MPL. Minimizing the occurrence of pinholes in these thin-film ionomer membranes will be achieved by optimizing the membrane thickness, optimizing the ionomer solvent parameters (i.e. viscosity, flow rate, stage temperature), or by utilizing smoother carbon paper substrates with fewer cracks in the microporous layer.

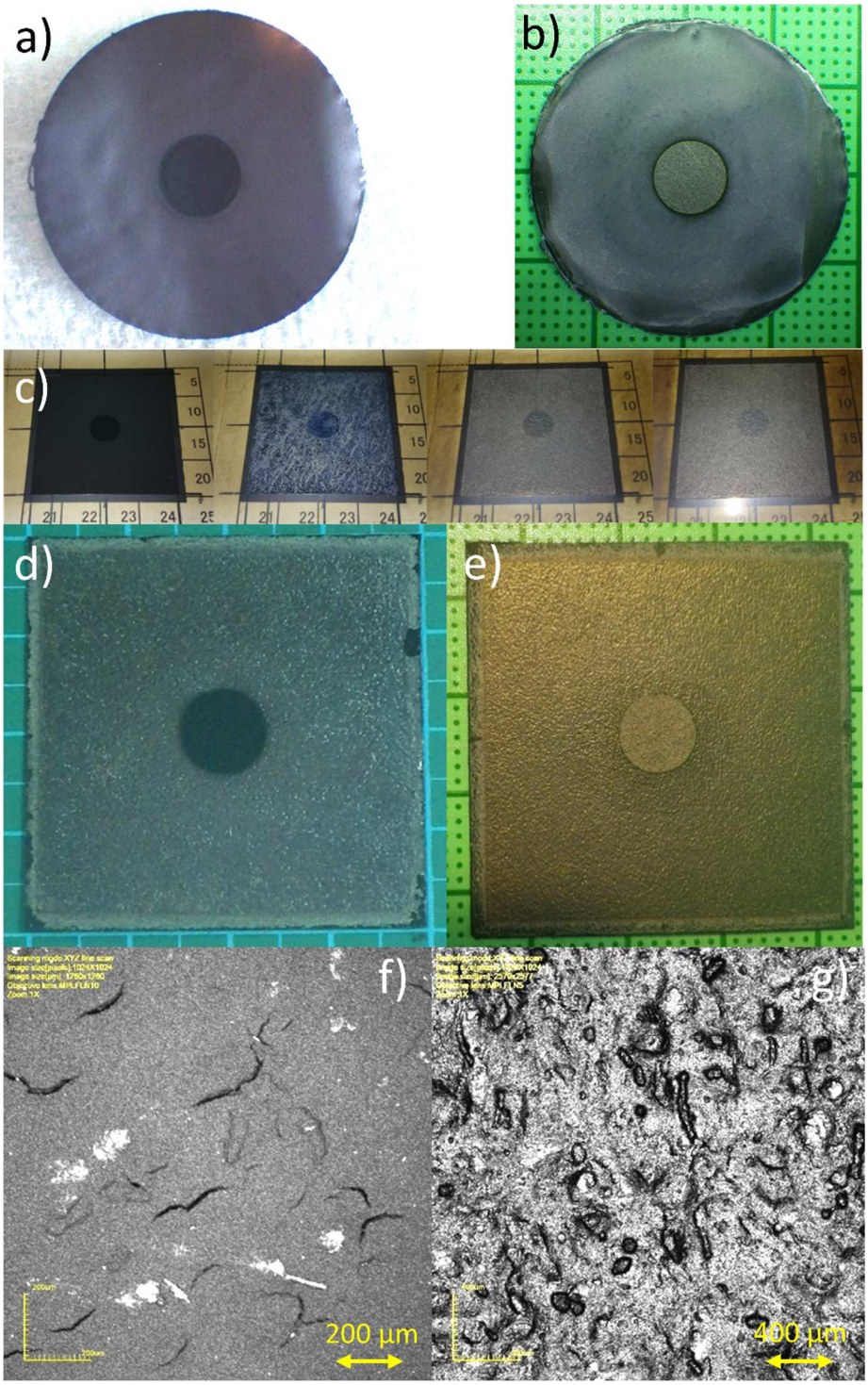

Figure 5. A GOMFC with conventional electrolyte-supported cell structure: (a) free-standing GO membrane sprayed with a Pt/C electrocatalyst layer, and (b) after attaching a carbon paper GDL. Spray-painted GOMFC with electrode-supported cell design: (c) carbon-paper GDL sprayed with Pt/C cathode electrocatalyst, and three successive GO spraying steps in which the electrolyte layer increases in

thickness; (d) Pt/C anode electrocatalyst sprayed onto the GO electrolyte; (e) final spray painted GOMFC with attached carbon paper GDL. Laser microscopy images of: (f) the carbon paper GDL, and (g) the sprayed GO surface.

Figure 6 shows SEM images of cross-sections of the conventionally fabricated electrolyte-supported GOMFCs (a) before and (b) after attaching the GDL. In the electrode-supported cell, the cathode electrocatalyst is sprayed onto the carbon paper (Figure 6c, bottom of image). The GO membrane spray-painted onto the cathode electrocatalyst is of uniform thickness (~5 μm in the device shown in Figure 6c, and ~3 μm in the device shown in 6d), indicating that spraying is a suitable method to fabricate uniform GO ionomer layers. In Figure 6d it can be seen that the GO membrane has approximately half the thickness of the anode electrocatalyst layer, which is sprayed on top of that. Figure 6e shows a large area where the cathode electrocatalyst has delaminated during razor blade cutting for sample preparation. However, despite this, the extremely thin GO membrane is still strong enough to support the anode electrocatalyst layer.

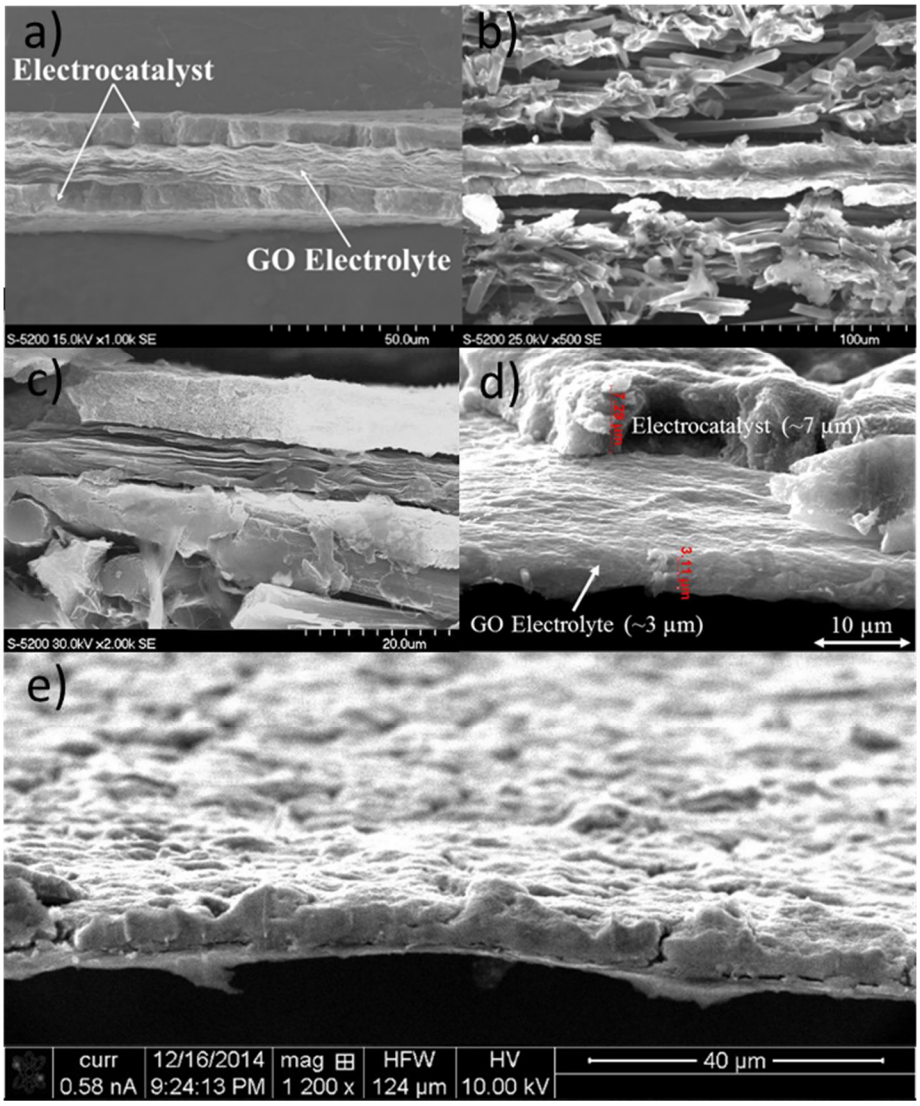

Figure 6. SEM cross-sectional images of electrolyte-supported GOMFCs (a) before, and (b) after attachment of the carbon paper GDL. Electrode-supported GOMFCs (c) sandwiched between the anode and cathode electrocatalyst layers, (d) showing the relative thickness of the electrolyte and electrocatalyst layers, and (e) showing a larger area of the electrolyte and anode, after delamination of the cathode.

Figure 7a shows the fuel cell performance for GOMFCs fabricated with GO membranes of different thickness, compared with a Nafion-membrane based PEMFC fabricated under similar conditions. Four different thicknesses of GO ionomer layers are investigated: 50, 16, 5, and 3 µm. The 50 and 16 µm membranes were prepared by vacuum filtration and the MEAs are membrane-supported. The 5 and 3 µm

membranes are fabricated by spray painting GO directly onto the cathode. To date we have not been able to successfully fabricate a working MEA using a Nafion membrane with a thickness of less than 10 μm, and this is seen as one of the major advantages of GO. The increased ability to form thin membranes may be due to the increased mechanical strength of GO, and/or the unique lamellar microstructure. For the 50 μm and 16 μm thick GO membranes, the open circuit voltage (OCV) is very high (~1.01 V). This suggests that the membrane is an almost pure proton conductor (since mixed ionic electronic conduction would lower the OCV), and that hydrogen crossover is negligible, (which would also lower the OCV). This confirms our previous work in which GO was shown to be a proton conductor at high humidity and room temperature (but a mixed ionic conductor at lower humidity / higher temperature) [30]. The negligible hydrogen crossover is attributed to the extremely low hydrogen permeability observed in Figure 3. However, for the 5 and 3 μm membranes the OCV is much lower, at 0.51 and 0.57 V, respectively. The ex-situ gas barrier properties of GO were shown to be high in gas barrier measurements and therefore only a slight decrease in OCV should be expected. However, as shown in the laser microscopy images (Figure 5g), the GO membrane potentially contains pinholes, which would result in increased gas crossover and thus reduced OCV due to the mixed potential. The OCV for the Nafion cell is 0.96 V.

The gradient of the I-V curves corresponds to the cell resistance (from Ohm's law), and this gradient increases significantly with decreasing thickness. This relationship is as expected, since the membrane resistance should decrease with decreasing thickness. The cell resistances for 50, 16, 5, and 3 μm are calculated from the I-V curves to be 43, 4.2, 0.62, and 0.89 Ω cm^2, respectively. This shows that the cell resistance can be improved not only by increasing the ionic conductivity, but also by simply reducing the membrane thickness, and that spray painting / printing could be ideal methods to achieve this. The 5 μm membrane has the lowest resistance, despite not being the thinnest membrane. This device also had the lowest OCV. Therefore it is postulated that this membrane has more pinholes, and that thinner areas of membrane around the pinholes contributes to lower membrane resistance. The cell resistance for the Nafion PEMFC is 0.64 Ω cm^2, similar to the 5 μm GOMFC.

The power density is obtained simply by multiplying the current and voltage. The maximum power density dramatically increases with decreasing thickness (Figure 7b,c). The membrane-supported GOMFC with a

50 µm has extremely low maximum power density of just 5.5 mW cm^{-2}, due to the high membrane and cell resistances. Decreasing the thickness to 16 µm increases the maximum power density to 33.8 mW cm^{-2} as the cell resistance decreases. The sprayed 5 and 3 µm spray-painted membranes have maximum power densities of 57 and 80 mW cm^{-2}, respectively. This dramatic increase in power density is due to the much lower cell resistance afforded by the decrease in thickness, and occurs despite the much lower OCV. This suggests that there is even further room for improvement in power density is the problem of OCV can be solved, and this is currently under investigation. The Nafion-based PEMFC has a maximum power density of ~150 mW cm^{-2}.

By fabricating very thin films we not only decrease the cell resistance, but also reduce the cost. For example in this case, the cost of a 3 µm sprayed GO membrane is calculated to be ~870 USD/m^2. Despite GO traditionally being seen as a prohibitively expensive nanomaterial, this is a similar price to conventional Nafion membranes. By further reducing the thickness, the cost will drop accordingly. Meanwhile, the price of GO is rapidly dropping with time, whilst the price of Nafion is relatively constant.

The durability is also an extremely important consideration for new PEMFC materials and is often overlooked. Here, durability measurements were performed on 50 and 3 µm GOMFCs with 100 mA constant load current, and the change in cell voltage was monitored (Figure 6d). Unfortunately, for both tested membranes, the cell voltage drops rapidly. In our previous work [39], we showed that this is largely a result of loss of oxygen functional groups in the reducing hydrogen atmosphere. Pei and Cheng et al. proposed three major mechanisms for the hydrogen-induced reduction of GO: 1) formation of water molecules and hydroxyl groups via the evolution of carbonyl pairs; 2) ether and epoxy groups form in the presence of hydrogen hydroxyl groups; and 3) removal of residual hydroxyl groups from the GO surface and edges with the formation of water [59]. The loss of oxygen groups results in the restoration of the highly conductive sp^2 carbon network, increasing the electronic conductivity of GO and resulting in an electronic short cut current flow through the membrane. As a result, cell voltage and thus performance of the GOMFC drops. One solution to this issue could be the introduction of a very thin protective Nafion layer at the anode side of the GO membrane. For the 50 µm membrane, the voltage drops from 0.61 to 0.16 V in 80 minutes, and for the 3 µm membrane the voltage drops from 0.43 V to 0.16 V in just 60 minutes.

The durability of the electrode-supported GOMFC is slightly worse than the electrolyte-supported GOMFC, possibly due to the fact that the formation of electronically conducting pathways along the reduced GO will form more quickly through a thin membrane.

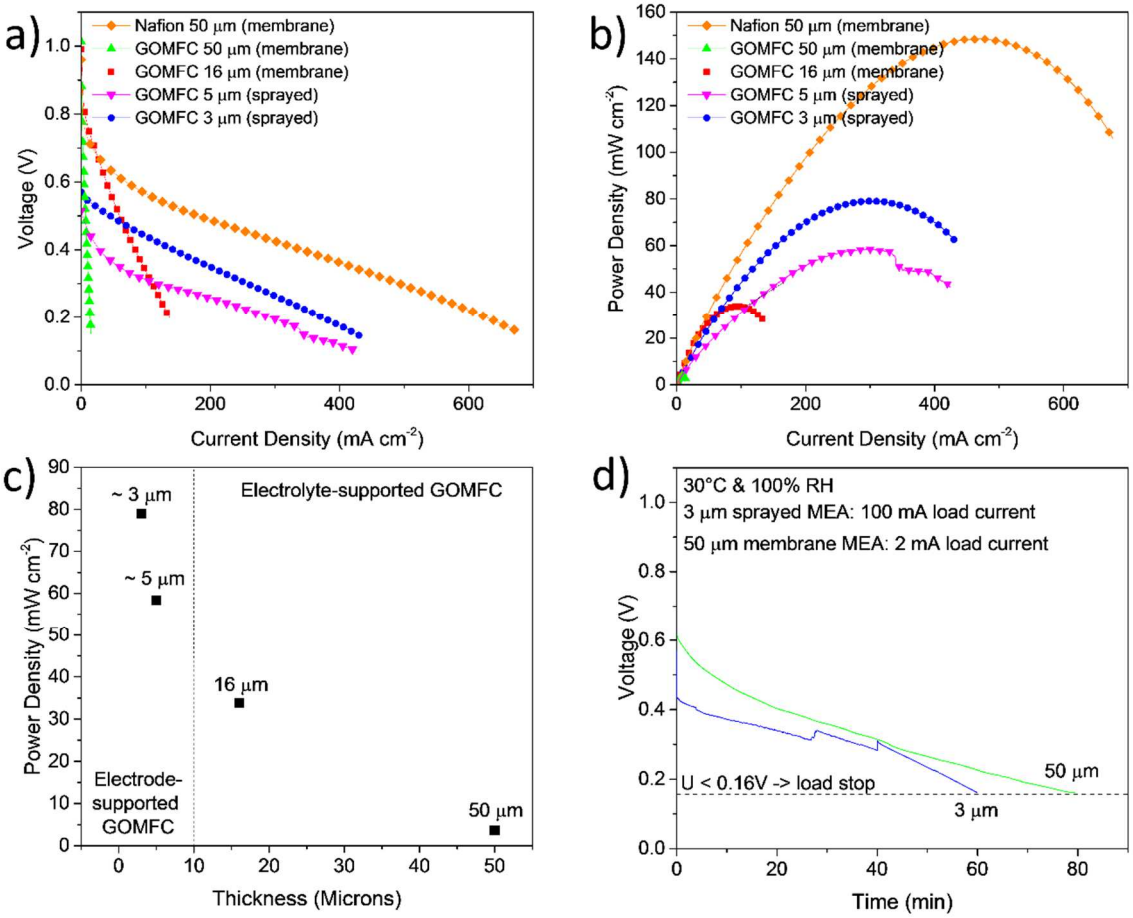

Figure 7. (a) Polarization I-V curves and (b) power density of electrolyte- and electrode-supported GOMFCs in comparison to a Nafion-based PEMFC. (c) Dependence of power density on electrolyte thickness showing the strong performance of electrode-supported GOMFCs. (d) Durability of a 3μm electrode-supported GOMFC and a 50μm membrane-supported GOMFC at constant load current.

4 Summary and Conclusions

We performed an investigation into the applicability of graphene oxide as a fuel cell ionomer membrane. Flexible graphene oxide membranes were fabricated by vacuum filtration. The hydrogen permeability was

measured to be 3 orders of magnitude lower than in Nafion. The proton conductivity of graphene oxide was investigated in detail, and an extremely high anisotropy was found between the in-plane (49.9 mS cm^{-1}) and through-plane (0.5 mS cm^{-1}) conductivities. The in-plane conductivity of GO was found to be comparable to the through-plane conductivity of Nafion. In order to take advantage of the extremely low hydrogen permeability and overcome the relatively low through-plane proton conductivity, we fabricated extremely thin graphene oxide membrane fuel cells (GOMFCs) by spray painting graphene oxide directly as an electrode-supported ionomer membrane. GOMFCs with membrane thickness varying from 50 to 3 μm were fabricated and characterized. The open circuit voltage (OCV) was very high for the thicker membrane due to pure proton conduction and low hydrogen crossover. However, the OCV was very low for the thinner sprayed membranes due to pinholes. The cell resistance decreased significantly with decreasing membrane thickness. The maximum power density also increased significantly with decreasing membrane thickness to ~80 mW cm^{-2}, despite the low OCV. This work suggests that decreasing the thickness of the ionomer membrane is a suitable method to increase fuel cell performance, especially in materials with low hydrogen permeability, provided that the presence of pinholes can be avoided.

5 Acknowledgements

The authors gratefully acknowledge the support of the International Institute for Carbon Neutral Energy Research (WPI-I2CNER), sponsored by the World Premier International Research Center Initiative (WPI), MEXT, Japan, the International Research Center for Hydrogen Energy at Kyushu University, the Japan Science and Technology Agency (JST) through its “Center of Innovation Science and Technology based Radical Innovation and Entrepreneurship Program (COI Program)”, and the Core Research for Evolutional Science and Technology (CREST) program from JST.

6 References

[1] D. Carter, J. Wing, The Fuel Cell Industry Review 2013, 2013.

[2] J. Liu, D. Takeshi, K. Sasaki, S.M. Lyth, Platinum-Decorated Nitrogen-Doped Graphene Foam Electrocatalysts, Fuel Cells. 14 (2014) 728–734.

[3] S.M. Lyth, H. Shao, J. Liu, K. Sasaki, E. Akiba, Hydrogen adsorption on graphene foam synthesized by combustion of sodium ethoxide, Int. J. Hydrogen Energy. 39 (2013) 376–380.

[4] Q. Li, R. He, J.O. Jensen, N.J. Bjerrum, Approaches and Recent Development of Polymer Electrolyte Membranes for Fuel Cells Operating above 100 °C, Chem. Mater. 15 (2003) 4896–4915.

[5] S.C. Yeo, A. Eisenberg, Physical properties and supermolecular structure of perfluorinated ion-containing (nafion) polymers, J. Appl. Polym. Sci. 21 (1977) 875–898.

[6] J.B. Kerr, G. Liu, X. Sun, New Polyelectrolyte Materials for High-Temperature Fuel Cells , Membrane Electrode Assemblies and Enhanced Selectivity, Prog. Rep. - DOE Hydrog. Progr. (2004) 366–372.

[7] M.B. Satterfield, P.W. Majsztrik, H. Ota, J.B. Benziger, A.B. Bocarsly, Mechanical Properties of Nafion and Titania / Nafion Composite Membranes for Polymer Electrolyte Membrane Fuel Cells, J. Polym. Sci. Part B Polym. Phys. 44 (2006) 2327–2345.

[8] N.H. Jalani, K. Dunn, R. Datta, Synthesis and characterization of Nafion®-MO2 (M=Zr, Si, Ti) nanocomposite membranes for higher temperature PEM fuel cells, Electrochim. Acta. 51 (2005) 553–560.

[9] C. Francia, V.S. Ijeri, S. Specchia, P. Spinelli, Estimation of hydrogen crossover through Nafion® membranes in PEMFCs, J. Power Sources. 196 (2011) 1833–1839.

[10] J. Ling, O. Savadogo, Comparison of Methanol Crossover among Four Types of Nafion Membranes, J. Electrochem. Soc. 151 (2004) 1604–1610.

[11] J. Liu, D. Takeshi, D. Orejon, K. Sasaki, S.M. Lyth, Defective Nitrogen-Doped Graphene Foam: A Metal-Free, Non-Precious Electrocatalyst for the Oxygen Reduction Reaction in Acid, J. Electrochem. Soc. 161 (2014) F544–F550.

[12] S.M. Lyth, Y. Nabae, N.M. Islam, T. Hayakawa, S. Kuroki, M. Kakimoto, et al., Solvothermal Synthesis of Nitrogen-Containing Graphene for Electrochemical Oxygen Reduction, eJournal Surf. Sci. Nanotechnol. 10 (2012) 29–32.

[13] X. Dong, C.-Y. Su, W. Zhang, J. Zhao, Q. Ling, W. Huang, et al., Ultra-large single-layer graphene obtained from solution chemical reduction and its electrical properties., Phys. Chem. Chem. Phys. 12 (2010) 2164–2169.

[14] D.-W. Wang, A. Du, E. Taran, G.Q. (Max) Lu, I.R. Gentle, A water-dielectric capacitor using hydrated graphene oxide film, J. Mater. Chem. 22 (2012) 21085–21091.

[15] S. Sen Gupta, V. Manoj Siva, S. Krishnan, T.S. Sreeprasad, P.K. Singh, T. Pradeep, et al., Thermal conductivity enhancement of nanofluids containing graphene nanosheets, J. Appl. Phys. 110 (2011) 084302.

[16] R.R. Nair, H.A. Wu, P.N. Jayaram, I. V. Grigorieva, A.K. Geim, Unimpeded Permeation of Water Through Helium-Leak-Tight Graphene-Based Membranes, Science (80-.). 335 (2012) 442–444.

[17] D.R. Dreyer, S. Park, C.W. Bielawski, R.S. Ruoff, The chemistry of graphene oxide., Chem. Soc. Rev. 39 (2010) 228–240.

[18] A. Lerf, H. He, M. Forster, J. Klinowski, Structure of Graphite Oxide Revisited, J. Phys. Chem. B. 5647 (1998) 4477–4482.

[19] D.A. Dikin, S. Stankovich, E.J. Zimney, R.D. Piner, G.H.B. Dommett, G. Evmenenko, et al., Preparation and characterization of graphene oxide paper, Nature. 448 (2007) 457–460.

[20] R.K. Joshi, P. Carbone, F.C. Wang, V.G. Kravets, Y. Su, I. V Grigorieva, et al., Precise and ultrafast molecular sieving through graphene oxide membranes, Science. 343 (2014) 752–754.

[21] V.A. Smirnov, V.P. Vasil, N.N. Denisov, Y. V Baskakova, V.A. Dubovitskii, Electric behavior of interlayer water in graphene oxide films, Chem. Phys. Lett. 648 (2016) 87–90.

[22] K. Scott, Ravikumar, Freestanding sulfonated graphene oxide paper: a new polymer electrolyte

for polymer electrolyte fuel cells, Chem. Commun. 48 (2012) 5584–5586.

[23] K. Hatakeyama, H. Tateishi, T. Taniguchi, M. Koinuma, T. Kida, S. Hayami, et al., Tunable Graphene Oxide Proton/Electron Mixed Conductor that Functions at Room Temperature, Chem. Mater. 26 (2014) 5598–5604.

[24] M.R. Karim, K. Hatakeyama, T. Matsui, H. Takehira, T. Taniguchi, M. Koinuma, et al., Graphene Oxide Nanosheet with High Proton Conductivity, J. Am. Chem. Soc. 135 (2013) 8097–8100.

[25] T. Szabó, O. Berkesi, P. Forgó, K. Josepovits, Y. Sanakis, D. Petridis, et al., Evolution of surface functional groups in a series of progressively oxidized graphite oxides, Chem. Mater. 18 (2006) 2740–2749.

[26] R. Kumar, M. Mamlouk, K. Scott, A Graphite Oxide Paper Polymer Electrolyte for Direct Methanol Fuel Cells, Int. J. Electrochem. 2011 (2011) 1–7.

[27] H. Zarrin, D. Higgins, Y. Jun, Z. Chen, M. Fowler, Functionalized Graphene Oxide Nanocomposite Membrane for Low Humidity and High Temperature Proton Exchange Membrane Fuel Cells, J. Phys. Chem. C. 115 (2011) 20774–20781.

[28] H. Tateishi, K. Hatakeyama, C. Ogata, K. Gezuhara, J. Kuroda, a. Funatsu, et al., Graphene Oxide Fuel Cell, J. Electrochem. Soc. 160 (2013) F1175–F1178.

[29] K. Hatakeyama, M.R. Karim, C. Ogata, H. Tateishi, A. Funatsu, T. Taniguchi, et al., Proton Conductivities of Graphene Oxide Nanosheets: Single, Multilayer, and Modified Nanosheets., Angew. Chem. Int. Ed. Engl. (2014) 6997–7000.

[30] T. Bayer, S.R. Bishop, N. Perry, K. Sasaki, S.M. Lyth, Tunable Mixed Ionic/Electronic Conductivity and Permittivity of Graphene Oxide Paper for Electrochemical Energy Conversion, ACS Appl. Mater. Interfaces. 8 (2016) 11466–11475.

[31] R. Kumar, C. Xu, K. Scott, Graphite oxide/Nafion composite membranes for polymer electrolyte fuel cells, RSC Adv. 2 (2012) 8777–8782.

[32] Z. Jiang, X. Zhao, Y. Fu, A. Manthiram, Composite membranes based on sulfonated poly(ether ether ketone) and SDBS-adsorbed graphene oxide for direct methanol fuel cells, J. Mater. Chem. 22 (2012) 24862–24869.

[33] C. Xu, Y. Cao, R. Kumar, X. Wu, X. Wang, K. Scott, A polybenzimidazole/sulfonated graphite oxide composite membrane for high temperature polymer electrolyte membrane fuel cells, J. Mater. Chem. 21 (2011) 11359–11364.

[34] C. Bao, Y. Guo, L. Song, Y. Hu, Poly(vinyl alcohol) nanocomposites based on graphene and graphite oxide: a comparative investigation of property and mechanism, J. Mater. Chem. 21 (2011) 13942–13950.

[35] A. Shukla, S.D. Bhat, V.K. Pillai, Simultaneous unzipping and sulfonation of multi-walled carbon nanotubes to sulfonated graphene nanoribbons for nanocomposite membranes in polymer electrolyte fuel cells, J. Memb. Sci. 520 (2016) 657–670.

[36] W. Gao, G. Wu, M.T. Janicke, D. a. Cullen, R. Mukundan, J.K. Baldwin, et al., Ozonated graphene oxide film as a proton-exchange membrane, Angew. Chemie - Int. Ed. 53 (2014) 3588–3593.

[37] G. Jiang, M. Goledzinowski, F.J.E. Comeau, H. Zarrin, G. Lui, J. Lenos, et al., Free-Standing Functionalized Graphene Oxide Solid Electrolytes in Electrochemical Gas Sensors, Adv. Funct. Mater. 26 (2016) 1729–1736.

[38] Du Pont, DuPont ™ Nafion PFSA Membranes NRE-211 and NRE-212 Perfluorosulfonic acid polymer, Prod. Inf. (2004) 1–6.

[39] T. Bayer, S.R. Bishop, M. Nishihara, K. Sasaki, S.M. Lyth, Characterization of a Graphene Oxide Membrane Fuel Cell, J. Power Sources. 272 (2014) 239–247.

[40] K.-D. Kreuer, S.J. Paddison, E. Spohr, M. Schuster, Transport in proton conductors for fuel-cell applications: simulations, elementary reactions, and phenomenology., Chem. Rev. 104 (2004) 4637–4678.

[41] N. Agmon, The Grotthuss mechanism, Chem. Phys. Lett. 50 (1995) 456–462.

[42] T. Daio, T. Bayer, T. Ikuta, T. Nishiyama, K. Takahashi, Y. Takata, et al., In-Situ ESEM and EELS Observation of Water Uptake and Ice Formation in Multilayer Graphene Oxide, Sci. Rep. 5 (2015) 11807.

[43] M. Klingele, M. Breitwieser, R. Zengerle, S. Thiele, Direct deposition of proton exchange membranes enabling high performance hydrogen fuel cells, J. Mater. Chem. A. 3 (2015) 11239–11245.

[44] T. Bayer, H.-C. Pham, K. Sasaki, S. Matthew, Spray deposition of Nafion membranes: Electrode-supported fuel cells, J. Power Sources. 327 (2016) 319–326.

[45] M. Breitwieser, T. Bayer, A. Büchler, R. Zengerle, S.M. Lyth, S. Thiele, A fully spray-coated fuel cell membrane electrode assembly using Aquivion ionomer with a graphene oxide / cerium oxide interlayer, J. Power Sources. 351 (2017) 145–150.

[46] Graphene Laboratories Inc., Graphene Oxide, Graphene-Supermarket.com. (2017) 2. https://graphene-supermarket.com/Highly-Concentrated-Graphene-Oxide-175-ml.html (accessed June 8, 2017).

[47] J.W. Suk, R.D. Piner, J. An, R.S. Ruoff, Mechanical properties of monolayer graphene oxide, ACS Nano. 4 (2010) 6557–6564.

[48] T. Bayer, B. V Cunning, R. Selyanchyn, M. Nishihara, S. Fujikawa, K. Sasaki, et al., Alkaline Anion Exchange Membranes based on KOH-treated Multilayer Graphene Oxide, J. Memb. Sci. 508 (2016) 51–61.

[49] K.R. Cooper, Progress Toward Accurate Through-Plane Membrane Resistance and Conductivity Measurement, ECS Trans. 25 (2009) 1–19.

[50] K. Momma, F. Izumi, VESTA 3 for three-dimensional visualization of crystal, volumetric and morphology data, J. Appl. Crystallogr. 44 (2011) 1272–1276.

[51] S. Matteucci, Y. Yampolskii, B. Freeman, I. Pinnau, Materials Science of Membranes for Gas and Vapor Separation, John Wiley & Sons Ltd., Chichester, UK, 2006.

[52] H.W. Kim, H.W. Yoon, S. Yoon, B.M. Yoo, B.K. Ahn, Y.H. Cho, et al., Selective Gas Transport Through Few-Layered Graphene and Graphene Oxide Membranes, Science (80-.). 342 (2013) 91–96.

[53] C.L. Gardner, A. V Anantaraman, Studies on ion-exchange membranes . II . Measurement of the anisotropic conductance of Nafion®, J. Electrochem. Soc. 449 (1998) 209–214.

[54] M. Casciola, G. Alberti, M. Sganappa, R. Narducci, On the decay of Nafion proton conductivity at high temperature and relative humidity, J. Power Sources. 162 (2006) 141–145.

[55] S. Ma, Z. Siroma, H. Tanaka, Anisotropic Conductivity Over In-Plane and Thickness Directions in Nafion-117, J. Electrochem. Soc. 153 (2006) 2274–2281.

[56] J. Köfinger, G. Hummer, C. Dellago, Single-file water in nanopores, Phys. Chem. Chem. Phys. 13 (2011) 15333–15728.

[57] C. Dellago, M.M. Naor, G. Hummer, Proton Transport through Water-Filled Carbon Nanotubes, Phys. Rev. Lett. 90 (2003) 105902.

[58] H. Matsui, Y. Ohhta, C. Iida, M. Horii, M. Tadokoro, Observation of Quasi-One Dimensional Proton Conductions, J. Phys. Soc. Japan. 79 (2010) 103601.

[59] S. Pei, J. Zhao, J. Du, W. Ren, H.-M. Cheng, Direct reduction of graphene oxide films into highly conductive and flexible graphene films by hydrohalic acids, Carbon N. Y. 48 (2010) 4466–4474.

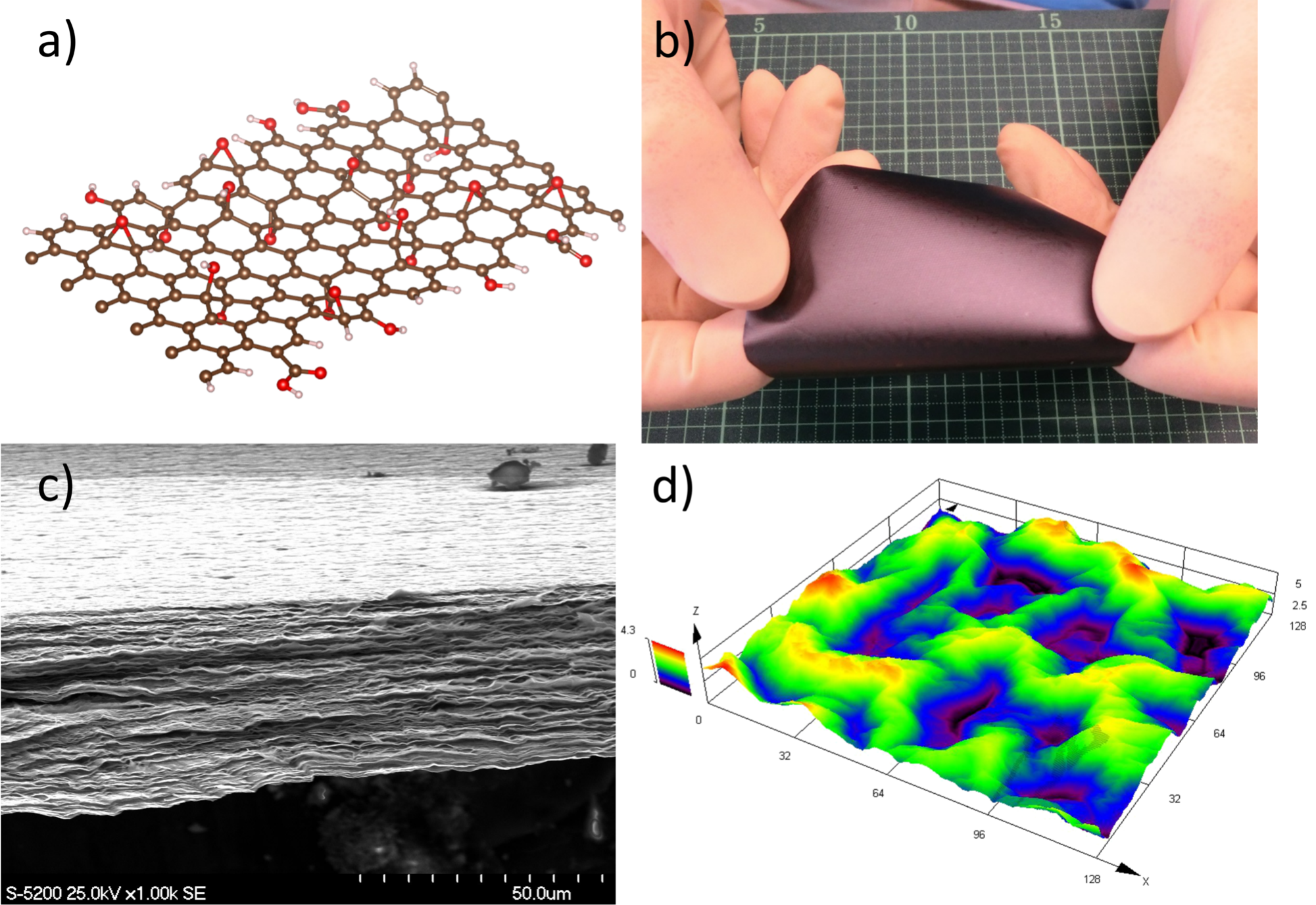
a)
b)
5
10
15
c)
S-5200 25.0kV x1.00k SE
50.0um
d)
Z
4.3
0
0
32
64
96
128
X
96
64
32
5
2.5
128

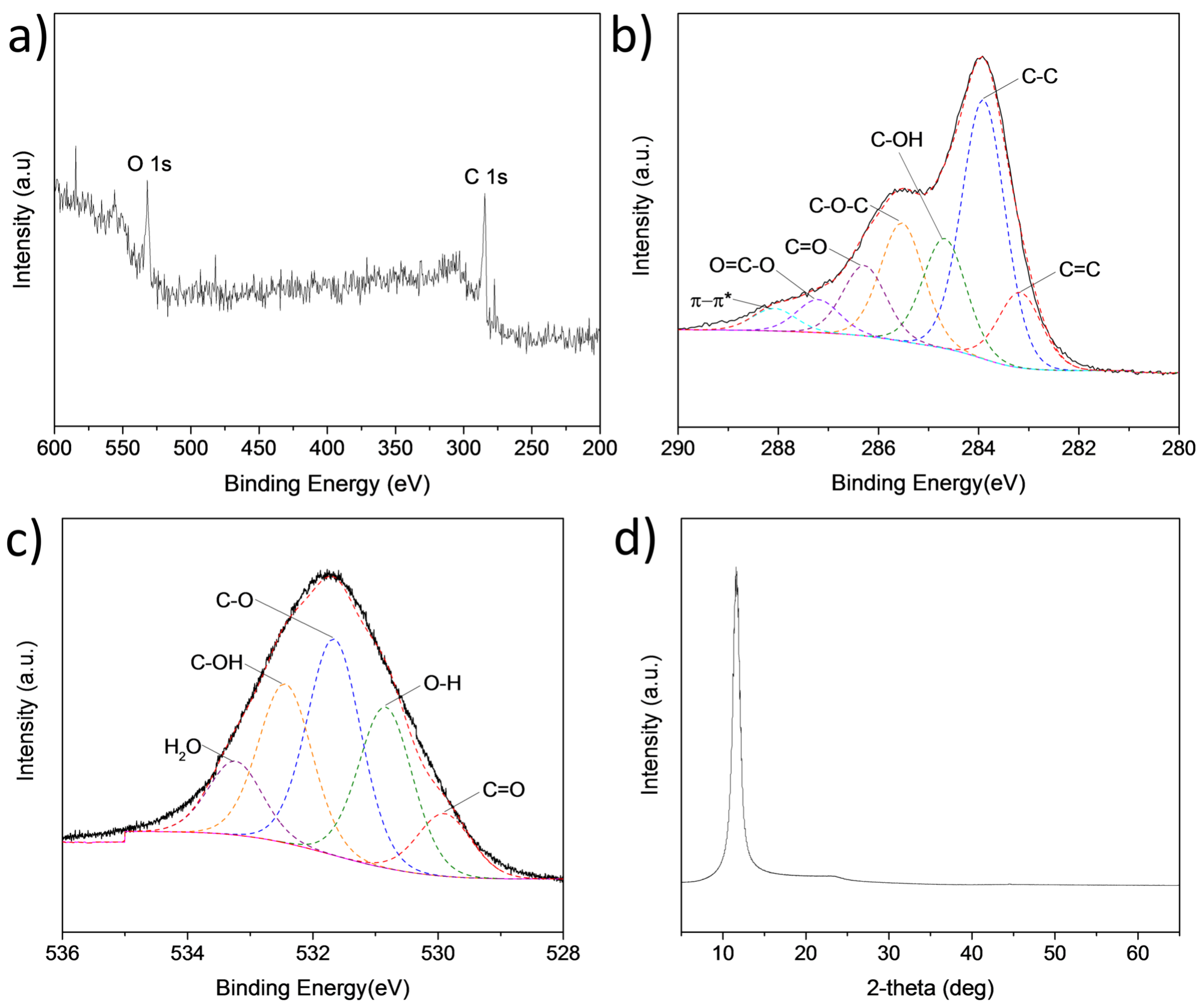
a)
O 1s
C 1s
Intensity (a.u)
600
550
500
450
400
350
300
250
200
Binding Energy (eV)
b)
C-C
C-OH
C-O-C
C=O
O=C-O
π–π*
C=C
Intensity (a.u.)
290
288
286
284
282
280
Binding Energy(eV)
c)
C-O
C-OH
O-H
H2O
C=O
Intensity (a.u.)
536
534
532
530
528
Binding Energy(eV)
d)
Intensity (a.u.)
10
20
30
40
50
60
2-theta (deg)

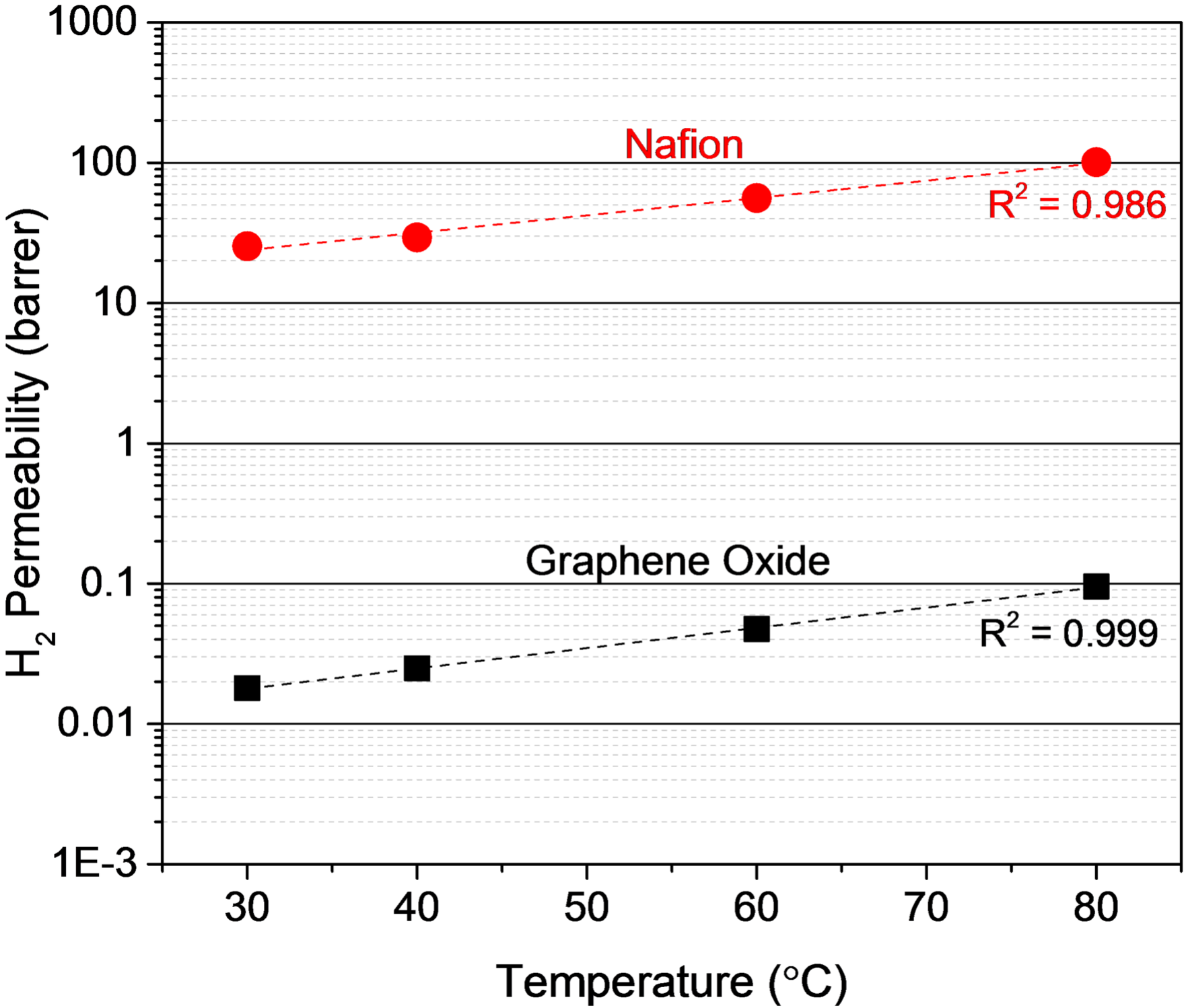
1000
100
10
1
0.1
0.01
1E-3
H2 Permeability (barrer)
Nafion
R2 = 0.986
Graphene Oxide
R2 = 0.999
30
40
50
60
70
80
Temperature (°C)

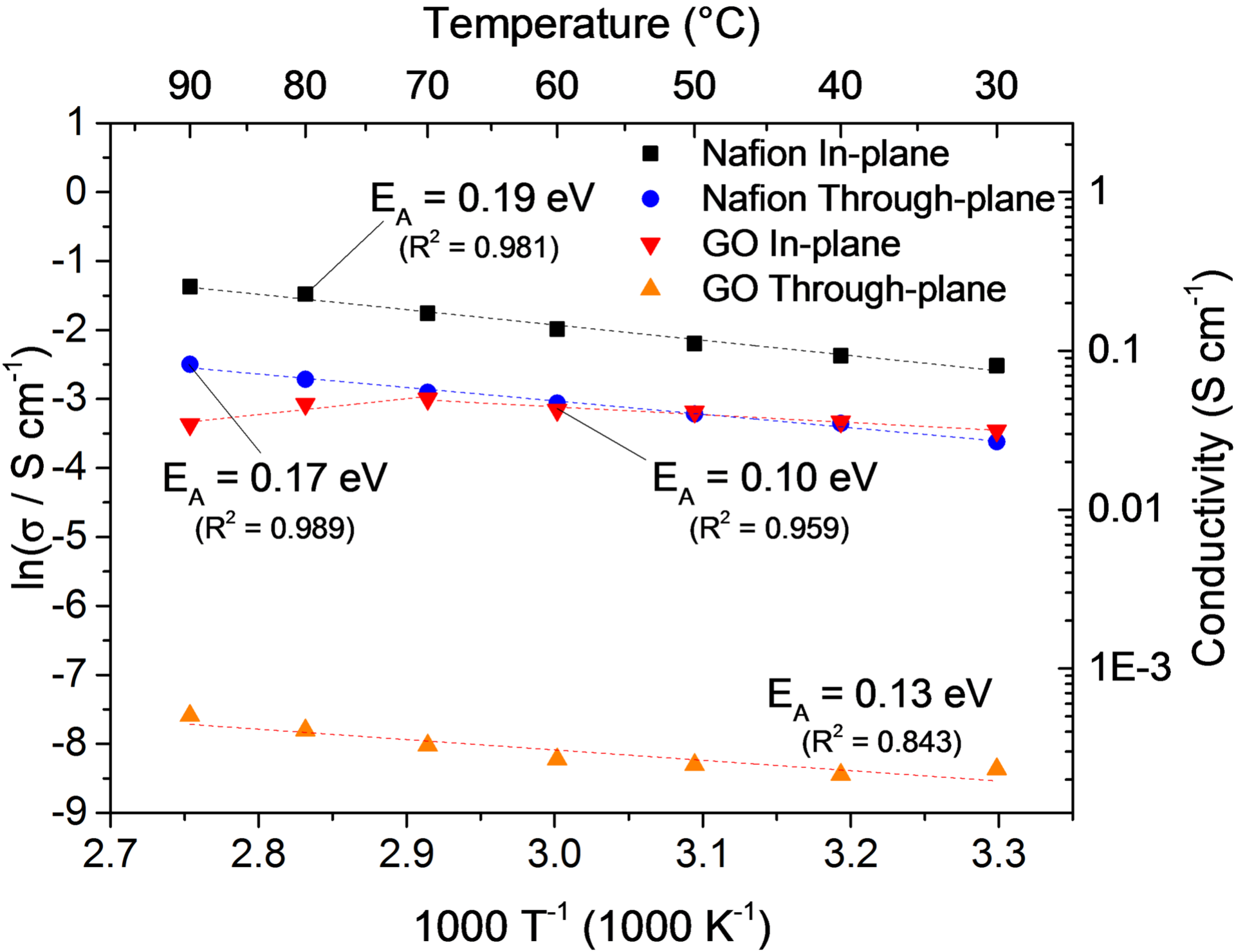
Temperature (°C)
90
80
70
60
50
40
30
1
0
-1
-2
-3
-4
-5
-6
-7
-8
-9
ln(σ / S cm-1)
Nafion In-plane
Nafion Through-plane
GO In-plane
GO Through-plane
EA = 0.19 eV
(R2 = 0.981)
EA = 0.17 eV
(R2 = 0.989)
EA = 0.10 eV
(R2 = 0.959)
EA = 0.13 eV
(R2 = 0.843)
1
0.1
0.01
1E-3
Conductivity (S cm-1)
2.7
2.8
2.9
3.0
3.1
3.2
3.3
1000 T-1 (1000 K-1)

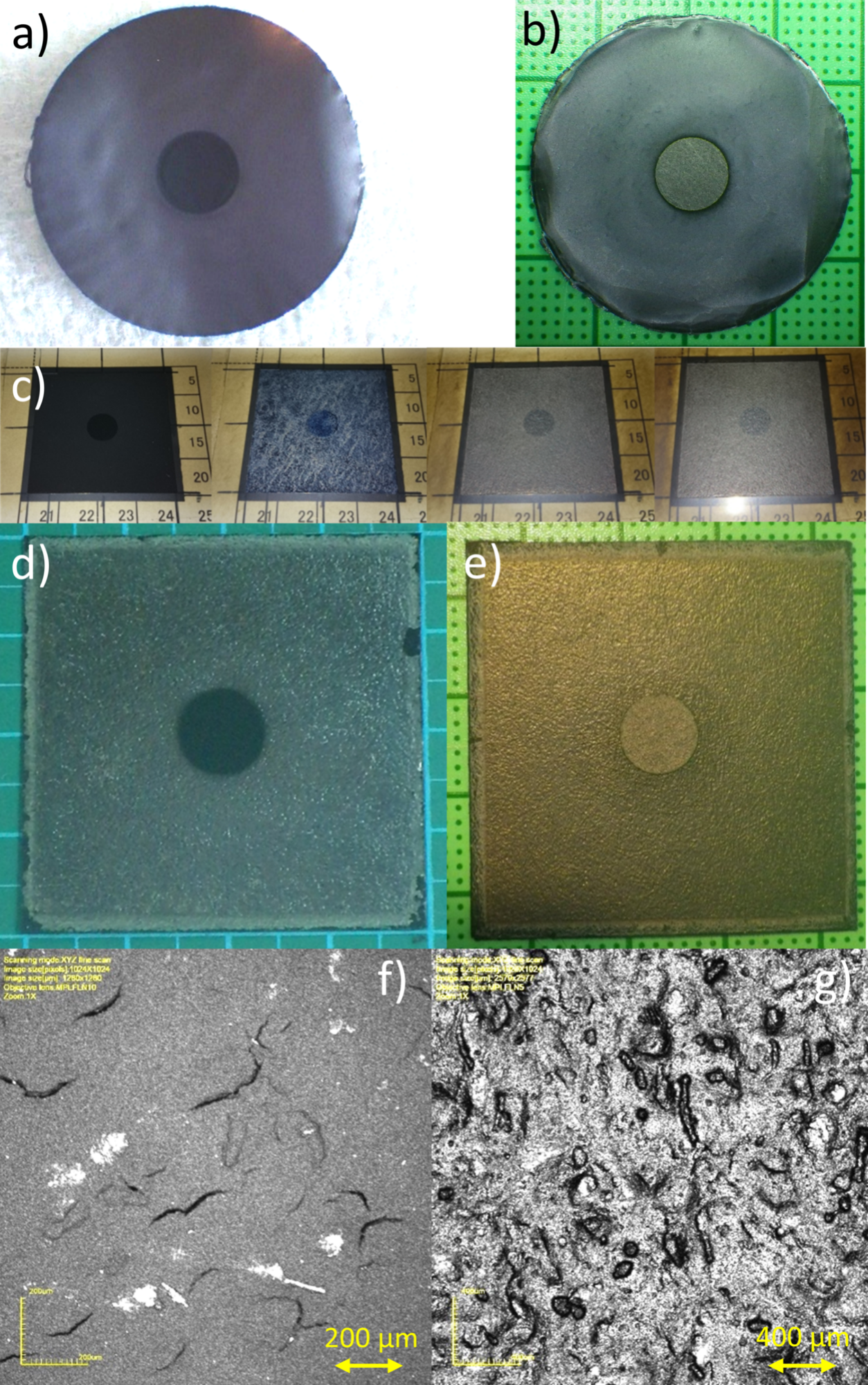
a)
b)
c)
d)
e)
f)
g)
200 µm
400 µm

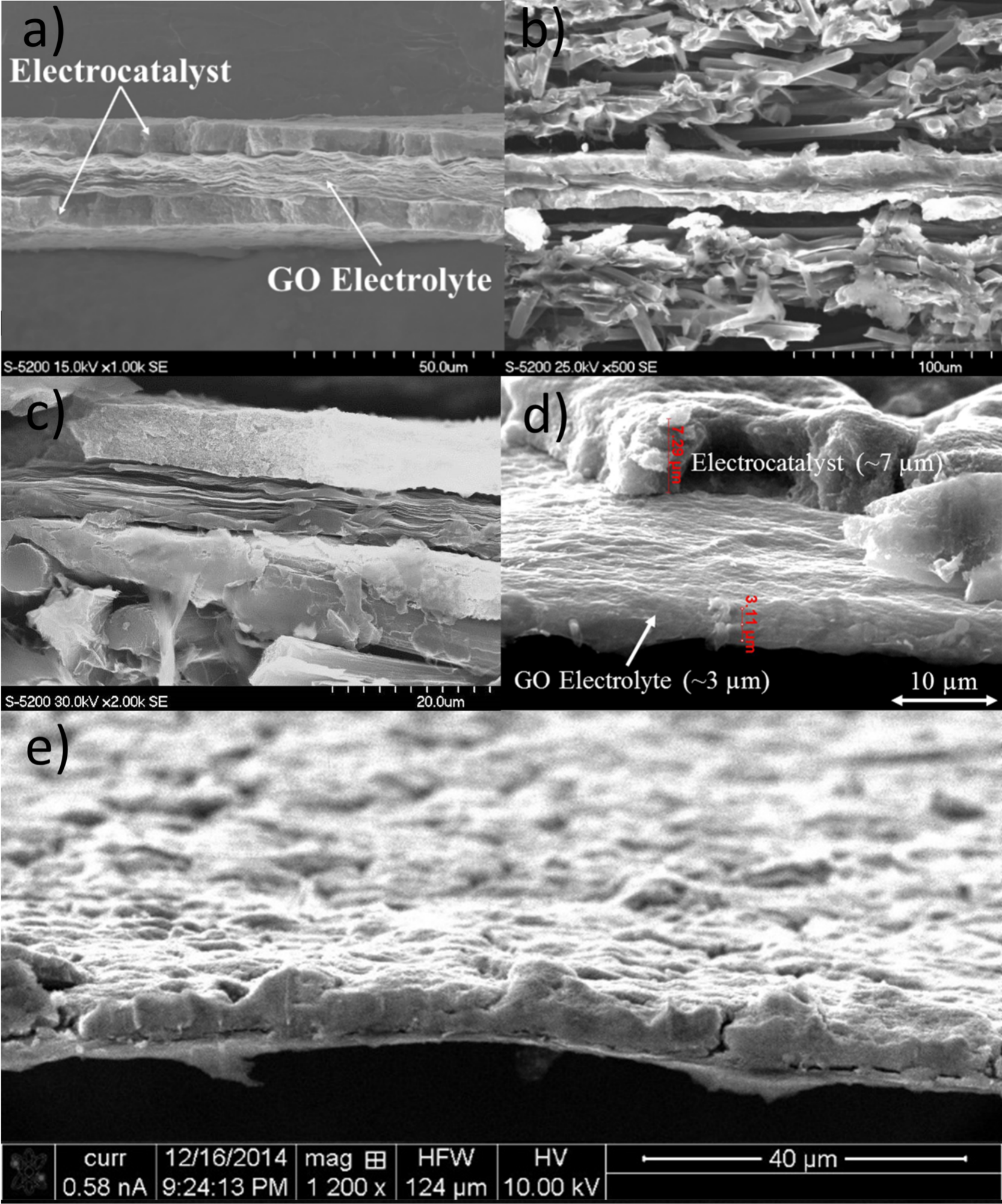
a)
Electrocatalyst
GO Electrolyte
S-5200 15.0kV x1.00k SE
50.0um
b)
S-5200 25.0kV x500 SE
100um
c)
S-5200 30.0kV x2.00k SE
20.0um
d)
7.29 µm
Electrocatalyst (~7 µm)
3.11 µm
GO Electrolyte (~3 µm)
10 µm
e)
curr
0.58 nA
12/16/2014
9:24:13 PM
mag
1 200 x
HFW
124 µm
HV
10.00 kV
40 µm

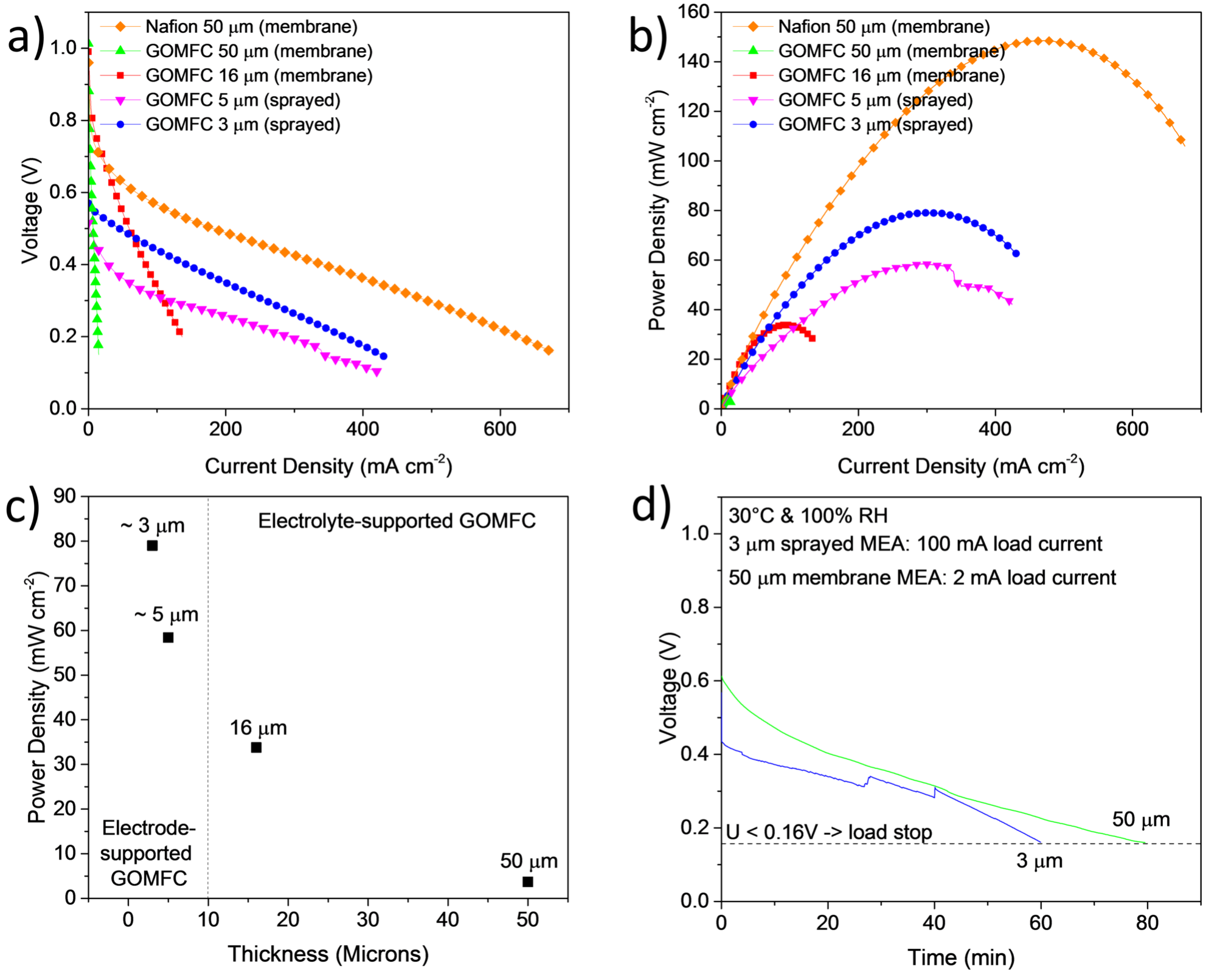
a)
Nafion 50 μm (membrane)
GOMFC 50 μm (membrane)
GOMFC 16 μm (membrane)
GOMFC 5 μm (sprayed)
GOMFC 3 μm (sprayed)
Voltage (V)
Current Density (mA cm-2)
b)
Power Density (mW cm-2)
c)
~ 3 μm
~ 5 μm
16 μm
50 μm
Electrolyte-supported GOMFC
Electrode-supported GOMFC
Thickness (Microns)
d)
30°C & 100% RH
3 μm sprayed MEA: 100 mA load current
50 μm membrane MEA: 2 mA load current
U < 0.16V -> load stop
Time (min)

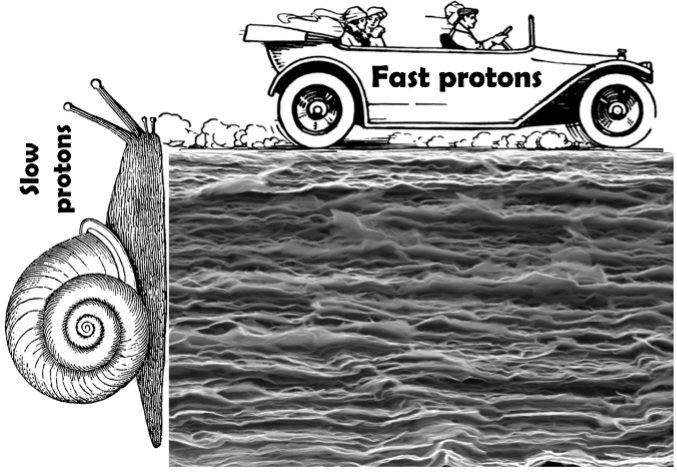
Fast protons
Slow protons

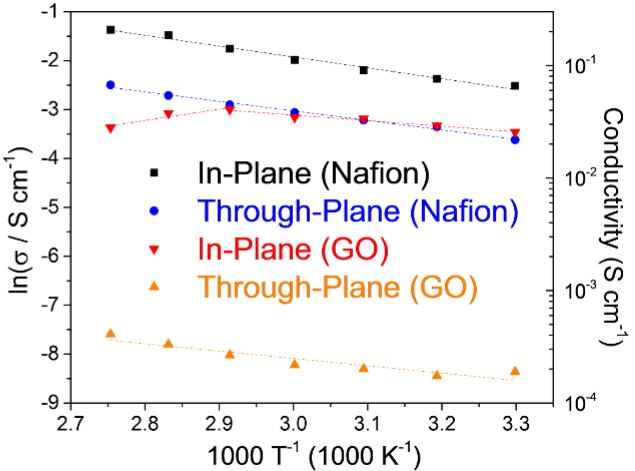
In-Plane (Nafion)
Through-Plane (Nafion)
In-Plane (GO)
Through-Plane (GO)
ln(σ / S cm-1)
Conductivity (S cm-1)
1000 T-1 (1000 K-1)
-1
-2
-3
-4
-5
-6
-7
-8
-9
10-1
10-2
10-3
10-4
2.7
2.8
2.9
3.0
3.1
3.2
3.3